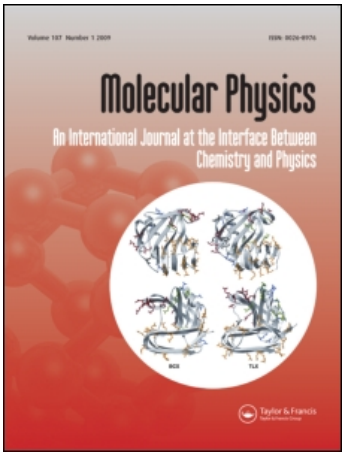

Molecular Physics
Publication details, including instructions for authors and subscription information:
http://www.informaworld.com/smpp/title~content=t713395160

Nuclear quadrupole resonance exchange spectroscopy with shaped radiofrequency pulses

Samanwita Pal[a]; N. Chandrakumar[a]
[a] Department of Chemistry, Indian Institute of Technology, Madras, Chennai, India

To cite this Article Pal, Samanwita and Chandrakumar, N.(2008) 'Nuclear quadrupole resonance exchange spectroscopy with shaped radiofrequency pulses', Molecular Physics, 106: 6, 759 — 767
To link to this Article: DOI: 10.1080/00268970801953796
URL: http://dx.doi.org/10.1080/00268970801953796

Molecular Physics
Vol. 106, No. 6, 20 March 2008, 759–767

Taylor & Francis
Taylor & Francis Group

RESEARCH ARTICLE

Nuclear quadrupole resonance exchange spectroscopy with shaped radiofrequency pulses

Samanwita Pal and N. Chandrakumar*

Department of Chemistry, Indian Institute of Technology, Madras, Chennai, 600036, India

(*Received 4 January 2008; final version received 28 January 2008*)

Recent work on the nuclear quadrupole resonance (NQR) investigation of molecular dynamics in the solid state has relied on 2D methods. We report our studies of dynamic processes by 1D shaped pulse NQR spectroscopy. Significant advantages include considerably shorter experimental duration, clear definition of the exchange time window, and avoidance of off-resonance effects. The reorientation of the $Cl_3\tilde{C}$ group in polycrystalline chloral hydrate [$Cl_3C–CH(OH)_2$] is considered as a test case. This may be modelled as a three-site exchange process. An analysis of the generalised Bloch–McConnell equation is performed to formulate the kinetic matrix. The present approach involves simultaneous excitation of the sites that undergo chemical exchange by employing a suitably modulated shaped RF pulse, followed by a mixing time, and finally a suitable read pulse for signal detection. The experimental signal intensities are plotted against the mixing time to extract the kinetic parameters, i.e. the exchange rate and the spin-lattice relaxation rate. Variable temperature measurements are carried out to determine the activation parameters. Short experiment times are possible in our 1D mode, enabling a large number of runs to be readily performed as a function of mixing time and temperature. The kinetic and activation parameters obtained in the case of chloral hydrate are in good agreement with recent literature values.

Keywords: molecular dynamics; solid state; NQR spectroscopy; modulated shaped pulses; multiply selective excitation

1. Introduction

Molecular dynamics such as internal rotation, reorientation of molecules as a whole, as well as self-diffusion are common in the solid state. From the perspective of a quadrupolar nucleus (spin $>1/2$), such molecular motion results in changes in the electric field gradient (EFG). The magnitude of the EFG is generally similar for the different states accessed during the dynamic process, but the orientation of the EFG principal axes for the particular nucleus changes sharply [1].

Dynamic processes involving quadrupolar nuclei in the solid state may be probed by NQR spectroscopy [2]. Measurement of line width [3], spin-lattice relaxation time [4,5] and the temperature dependence of the resonance frequency [6] reveals molecular motion such as the reorientation of a molecular group. Over the years, 1D experiments were used to measure the NQR spin-lattice relaxation time and resonance frequency as a function of temperature. In the last decade, 2D NQR exchange experiments [7–11] based on Jeener *et al*'s three-pulse sequence [12] have attracted considerable attention.

Two-dimensional experiments permit intuitive visualisation of the exchange network. However, major concerns in 2D experiments, besides the experimental duration, are the excitation efficiency, off-resonance effects as well as a clear definition of the 'exchange window' in the time domain experiment. Here we report the extension to solid-state NQR of the shaped pulse 1D approach developed to study chemical exchange in solution by NMR [13,14]. This strategy is justified by the known equivalence of a spin-3/2 in zero field to two fictitious spin-1/2 [15,16] and thence the applicability to NQR of shaped pulses designed for NMR [17–19]. Among the primary outcomes of our approach is the clear definition of the time window during which the dynamic process occurs, besides eliminating off-resonance effects as well as reducing the duration of the experiment.

The basic features of NQR exchange that distinguish it from its NMR counterpart may be recounted as follows.

(1) Besides the resonance frequency, the axis of quantisation changes its direction due to the specific dynamic process, since the axis of nuclear spin quantisation is governed, in zero field NQR, by the principal axis of the EFG tensor [1,7].

*Corresponding author. Email: nckumar@iitm.ac.in

ISSN 0026–8976 print/ISSN 1362–3028 online

DOI: 10.1080/00268970801953796
http://www.informaworld.com

(2) EFGs change non-adiabatically, the exchange processes being considered as 'sudden jumps' [1] with negligible transition time: this results in a polarisation loss.
(3) The NQR signal intensity depends on the orientation of the RF coil axis [20] with respect to the quadrupolar principal axis system (QPAS). Hence, for powdered samples, we have to consider corresponding powder averages.
(4) The spectral width is spread over several hundred kHz; hence, off-resonance excitation is often an issue in NQR that could lead to signal loss.

In the following we will describe the method developed involving simultaneous multi-site excitation employing pulses that are multiply selective to overcome the off-resonance effect. In the present work, we consider a three-site exchange process such as reorientation of the $Cl_3C–$ group [2,7–11] in chloral hydrate [21]. A detailed description of the corresponding Bloch–McConnell equations [22] and the complete density matrix calculation for the pulse sequence following Goldman's fictitious spin-1/2 formalism [16] is given. Experimental results are reported, analysed and compared with the literature.

2. The pulse sequence

Two different pulse sequences were implemented to monitor both two- and three-site exchange processes in NQR. While a phase alternated train of pulses has been employed in the literature to irradiate at two relevant frequencies [7], our approach involves selective and bi-selective amplitude modulated shaped pulses [13,14]. Bi-selective shaped pulses are generated by appropriate amplitude modulation to achieve simultaneous two-site excitation of the exchanging sites. These pulses were previously employed for exchange studies in solution by NMR. Suitable pulse shape modulation schemes would, in principle, also permit multi-site excitation, provided the relevant NQR resonance frequencies comply with hardware bandwidth limitations. The present pulse sequences employed may be written as

$$1.\ (\Theta)_{\text{selective}} - \tau_m - (\Theta')_{\text{bi-selective}},$$

$$2.\ (\Theta)_{\text{bi-selective}} - \tau_m - (\Theta')_{\text{bi-selective}}.$$

The first sequence involves a Gaussian pulse that selectively 'inverts' one of the exchanging sites depending on the choice of carrier frequency. The second sequence involves a cosine modulated Gaussian pulse that simultaneously 'inverts' both the exchanging sites in the case of a two-site exchange process and two of the exchanging sites in the case of a multi-site exchange process. In both cases the read pulse is a cosine modulated bi-selective Gaussian pulse.

In both cases the first pulse creates non-equilibrium polarisation along the z-axis of the local QPAS. During the mixing period (τ_m) the 'inverted' polarisation is subject to both spin-lattice relaxation as well as exchange.

In powder NQR of an $I = 3/2$ spin with $\eta = 0$, an ideal '180°' pulse produces a 65% inversion of polarisation – besides a small amount of transverse polarisation, the precise amplitude of which also depends on the asymmetry parameter of the EFG [16]. Due to B_1 inhomogeneity the amount of transverse polarisation could be even higher. This could interfere with the signal intensity measured during acquisition. We therefore alternated the first pulse phase keeping the phase of the read pulse and that of the receiver constant to nullify this effect in a two-scan procedure. The phase cycle is given in Table 1.

3. Theoretical description

The pulse sequences were treated in terms of Goldman's fictitious spin-1/2 formalism [16] and the density matrix calculation is given below for both pulse sequences.

3.1. *NQR signal after a single pulse*

In order to put the results in perspective, we briefly recount below the established results for the NQR signal following a single pulse applied to a single spin-3/2 [16]. The signal intensity depends on the orientation of the RF coil with respect to the QPAS of the EFG tensor [20] at a particular crystal orientation. The polarisation is created along the z axis of QPAS. Since, for powder samples, all possible orientations of the microcrystallites are equally probable, powder averaging must be performed

Table 1. Phase cycle used for the selective and bi-selective inversion recovery experiments.

Scan	Θ	Θ'	Receiver
1	0	0	0
2	2	0	0

to generate the signal intensity. In terms of the Goldman formalism, the equilibrium polarisation is given as

$$\sigma_{eq} = z_1. \tag{1}$$

After a single rectangular pulse of duration t_p (issued with coil axis X) the density matrix takes the form

$$\sigma(0) = z_1 \cos(\lambda\Theta) - y_1 z_2' \sin(\lambda\Theta). \tag{2}$$

Here, $\lambda\Theta$ is the pulse flip angle and $x_1, y_1, \ldots, z_2$ are Pauli operators defined as follows:

$$x_1 = 2S_{1x}, \qquad x_2 = 2S_{2x}, \tag{3}$$

$$y_1 = 2S_{1y}, \qquad y_2 = 2S_{2y}, \tag{4}$$

$$z_1 = 2S_{1z}, \qquad z_2 = 2S_{2z}. \tag{5}$$

λ is the orientation factor, which depends on η, the asymmetry parameter, as well as the orientation of the RF coil with respect to the QPAS,

$$3\lambda^2 = \frac{[3(1-(\eta^2/3))(p^2+q^2) + 2\eta(p^2-q^2) + (4/3)\eta^2]}{(1+(\eta^2/3))}, \tag{6}$$

where p and q are given in terms of angles θ and φ as defined in Figure 1; we have

$$\begin{aligned} p &= \sin\theta\cos\phi, \\ q &= \sin\theta\sin\phi. \end{aligned} \tag{7}$$

The primed operator refers to the component of the fictitious spin in the direction corresponding to the resultant interaction, i.e. an effective 'field' direction. The density matrix during acquisition is given by

$$\sigma(t) = -z_2' \sin(\lambda\Theta)(y_1 \cos\delta t - x_1 \sin\delta t) + z_1 \cos(\lambda\Theta), \tag{8}$$

where t is the acquisition time and δ is the resonance offset. The polarisation along the transverse axis leads to the observed signal. For a single crystal considering the receiver coil along the laboratory X axis and taking the appropriate trace, the signal of interest for a particular RF coil orientation (θ, ϕ) relative to QPAS is given by the following expression with a suitable choice of phase:

$$S_{crystal} \propto \frac{\sqrt{3}}{2}\lambda \sin\lambda\Theta. \tag{9}$$

This is valid for the on-resonance case. On the other hand, for a polycrystalline sample, for the on-resonance case, the observed signal intensity is given by the following powder average:

$$S_{powder} = \frac{1}{4\pi}\int_0^{2\pi} d\phi \int_0^{\pi} d\theta \sin\theta \left(\frac{\sqrt{3}}{2}\lambda \sin\lambda\Theta\right), \tag{10}$$

where $\Theta = \sqrt{3}\gamma B_1 t_p$ is the nominal pulse flip angle, γ the gyromagnetic ratio, B_1 the RF field strength and t_p the pulse duration.

The signal intensity may be plotted as a function of the nominal pulse flip angle, from which we can find the maximum and minimum signal intensities and the corresponding nominal pulse flip angles. Table 2 gives the signal intensity after a single pulse for the two cases $\eta = 0$ and $\eta = 1$ as plotted by Goldman [16].

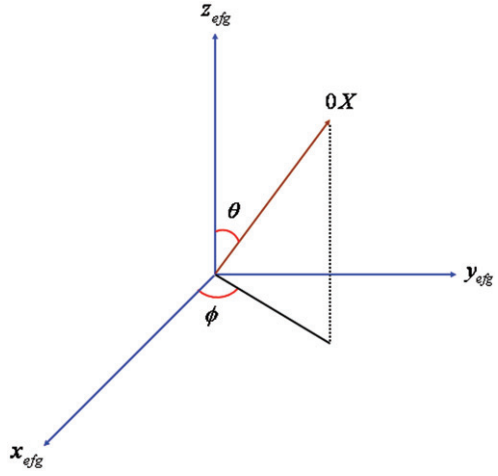

Figure 1. Orientation of the RF coil axis with respect to the QPAS.

3.2. *The Bloch–McConnell equations and kinetic matrix*

A detailed analysis of the generalised Bloch–McConnell-type equations [22] is given here to formulate the kinetic matrix for a three-site exchange process, the exchange network being defined in Figure 2.

Table 2. Theoretical intensities after a single pulse.

	Transverse component		Longitudinal component	
Θ	$\eta = 0$	$\eta = 1$	$\eta = 0$	$\eta = 1$
1.727[a]	0.74845	0.75202	0.07382	0.09567
3.629[b]	0.00002	0.07036	−0.65551	−0.62965

Notes: [a]$\Theta = 1.727$ corresponds to a '$\pi/2$' pulse.
[b]$\Theta = 3.6295$ corresponds to a 'π' pulse.

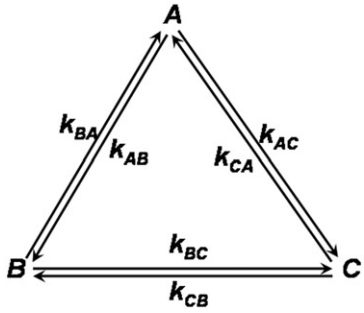

Figure 2. The three-site exchange network.

The Bloch–McConnell equations for such a system may be written as follows:

$$\frac{dz_{1A}(t)}{dt} = -\frac{(z_{1A}(t) - z_{1A})}{T_1} - (k_{AB} + k_{AC})z_{1A}(t) + r(k_{BA}z_{1B}(t) + k_{CA}z_{1C}(t)), \quad (11)$$

$$\frac{dz_{1B}(t)}{dt} = -\frac{(z_{1B}(t) - z_{1B})}{T_1} - (k_{BA} + k_{BC})z_{1B}(t) + r(k_{AB}z_{1A}(t) + k_{CB}z_{1C}(t)), \quad (12)$$

$$\frac{dz_{1C}(t)}{dt} = -\frac{(z_{1C}(t) - z_{1C})}{T_1} - (k_{CA} + k_{CB})z_{1C}(t) + r(k_{BC}z_{1B}(t) + k_{AC}z_{1A}(t)). \quad (13)$$

Here we have considered that all three sites (A, B, C) have the same spin-lattice relaxation time T_1 and reduction factor r, k_{ij} indicates the rate constant for the transfer from site i to site j, and the terms in k with negative sign denote outgoing polarisation, while the terms in k with positive sign denote incoming polarisation. A notable difference between NMR and NQR exchange is that the incoming polarisation in the case of NQR is associated with a term 'r' known as the 'reduction factor' [1]. In NQR when a nucleus leaves a site, the corresponding polarisation is lost at that site; however, when a nucleus enters another site, only a fraction of its polarisation 'arrives' at the destination site. This is because we consider a projection of the initial spin polarisation axis of the nucleus on the new one. This has been termed 'projection loss' and is a direct consequence of the fact that the EFG tensors change non-adiabatically [1]. The reduction factor depends on the structure of the molecule and the asymmetry parameter (η) associated with the quadrupolar nuclei of interest. The reduction factor for spin-3/2 is given as [10]

$$r = \frac{1}{2}[3\cos^2\beta - 1 + \eta\sin^2\beta], \quad (14)$$

where β is the angle between the z axes of the QPAS of the exchanging nuclei.

Replacing the individual rate constants by $k_{ij} = k[x_i]$ (with $i, j = $ A, B, C) where k is an average rate constant, $[x_i]$ the population of site i and invoking microscopic reversibility at dynamic equilibrium [8], the above set of differential equations may be formulated in terms of the following matrix representation:

$$\frac{d}{dt}\begin{bmatrix} L \\ M \\ N \end{bmatrix} = \begin{bmatrix} -\frac{1}{T_1} - \frac{2}{3}k & \frac{1}{3}rk & \frac{1}{3}rk \\ \frac{1}{3}rk & -\frac{1}{T_1} - \frac{2}{3}k & \frac{1}{3}rk \\ \frac{1}{3}rk & \frac{1}{3}rk & -\frac{1}{T_1} - \frac{2}{3}k \end{bmatrix}\begin{bmatrix} L \\ M \\ N \end{bmatrix}. \quad (15)$$

Here we have defined

$$L(t) = z_{1A}(t) - z_{1A},$$
$$M(t) = z_{1B}(t) - z_{1B},$$
$$N(t) = z_{1C}(t) - z_{1C}, \quad (16)$$

and considered equally populated sites

$$x_A = x_B = x_C = \frac{1}{3}. \quad (17)$$

The solution of the above set of coupled homogeneous differential equations may be given as

$$L(t) = \frac{1}{3}(2e - f - g)\exp[-(a + b)t] + \frac{1}{3}(e + f + g)\exp[-(a - 2b)t], \quad (18a)$$

$$M(t) = \frac{1}{3}(-e + 2f - g)\exp[-(a + b)t] + \frac{1}{3}(e + f + g)\exp[-(a - 2b)t], \quad (18b)$$

$$N(t) = \frac{1}{3}(-e - f + 2g)\exp[-(a + b)t] + \frac{1}{3}(e + f + g)\exp[-(a - 2b)t], \quad (18c)$$

where e, f, g define the initial conditions:

$$e = L(0) = z_{1A}(0) - z_{1A}, \quad (19a)$$

$$f = M(0) = z_{1B}(0) - z_{1B}, \quad (19b)$$

$$g = N(0) = z_{1C}(0) - z_{1C}, \quad (19c)$$

$$a = \left(\frac{1}{T_1} + \frac{2}{3}k\right), \quad b = \frac{1}{3}rk. \quad (20)$$

3.3. *Density matrix calculation for selective and bi-selective experiments*

3.3.1. *Sequence 1*

In the selective inversion experiment, any one of the three sites may be selectively inverted. In this context we place the spectrometer offset frequency at the middle of the two signals from sites A and B. The carrier frequency of the selective shaped pulse is then shifted to excite either site A or site B alone. Bi-selective excitation pulses, on the other hand, perturb both sites A and B, by employing a suitable modulation at a frequency that is one-half the frequency difference between the signals from the two sites A and B. At the end of the pulse sequence we observe signals from sites A and B. Site C remains unperturbed as well as unobserved: in our experimental system of chloral hydrate, this site has a resonance frequency that is 1.231 MHz lower than the average of the A and B site resonance frequencies.

The equilibrium spin density matrix for the system may be expressed as the tensor sum of the individual density matrices of the three sites:

$$\sigma_{eq} = \sigma_{A,eq} \oplus \sigma_{B,eq} \oplus \sigma_{C,eq}, \tag{21}$$

where $\sigma_{A,eq}$, $\sigma_{B,eq}$ and $\sigma_{C,eq}$ are the equilibrium spin density matrices for sites A, B and C respectively.

In the case of the singly selective inversion experiment (sequence 1), the RF pulse is assumed to be applied along the laboratory X direction, selectively inverting site A only. The spin density matrix immediately after the pulse is

$$\begin{aligned}\sigma(0) &= \sigma_A(0) \oplus \sigma_B(0) \oplus \sigma_C(0) \\ &= z_{1A}\cos\lambda\Theta - y_{1A}z'_{2A}\sin\lambda\Theta \oplus z_{1B} \oplus z_{1C}.\end{aligned} \tag{22}$$

Here, $\sigma_A(0)$ is written following Equation (2) where the first term is the polarisation created along the z axis of QPAS and is subjected to both spin-lattice relaxation (T_1) and the exchange process during the mixing period (τ_m), the second term being removed by phase cycling. Sites B and C remain unperturbed by the first pulse.

Polarisation at site A after the mixing period is given by

$$\sigma_A(\tau_m) = z_{1A}(\tau_m) = z_{1A} * P, \tag{23}$$

$$\begin{aligned}P = 1 &+ \frac{2}{3}(\cos\lambda\Theta - 1)\exp[-(a+b)\tau_m] \\ &+ \frac{1}{3}(\cos\lambda\Theta - 1)\exp[-(a-2b)\tau_m].\end{aligned} \tag{24}$$

The above result may be obtained by inserting the appropriate initial conditions into the solutions given by Equation (18):

$$e = z_{1A}(0) - z_{1A} = z_{1A}(\cos\lambda\Theta - 1), \tag{25}$$

where $z_{1A}(0)$ is the longitudinal polarisation just after the first pulse. On the other hand, since the other two sites are not inverted by the first pulse the initial conditions are the following:

$$f = z_{1B}(0) - z_{1B} = 0, \tag{26}$$

$$g = z_{1C}(0) - z_{1C} = 0. \tag{27}$$

The density matrix after the mixing period for the un-inverted sites is given as

$$\sigma_{B,C}(\tau_m) = z_{1B,C}(\tau_m) = z_{1B,C} * Q, \tag{28}$$

$$\begin{aligned}Q = 1 &- \frac{1}{3}(\cos\lambda\Theta - 1)\exp[-(a+b)\tau_m] \\ &+ \frac{1}{3}(\cos\lambda\Theta - 1)\exp[-(a-2b)\tau_m].\end{aligned} \tag{29}$$

The final density matrix leading to the signal after the second pulse is given by

$$\sigma_A(\tau_{m,+}) = P[z_{1A}\cos\lambda\Theta' - y_{1A}z'_{2A}\sin\lambda\Theta'], \tag{30}$$

$$\sigma_B(\tau_{m,+}) = Q[z_{1B}\cos\lambda\Theta' - y_{1B}z'_{2B}\sin\lambda\Theta']. \tag{31}$$

The final signal has contributions only from sites A and B since the second pulse is bi-selective to the sites A and B. Site C remains undetected.

Hence for a single crystal the signals of interest for inverted and un-inverted sites are as follows:

$$S_{Inv,crystal}(t) \propto \frac{\sqrt{3}}{2}\lambda P\sin\lambda\Theta', \tag{32}$$

$$S_{Uninv,crystal}(t) \propto \frac{\sqrt{3}}{2}\lambda Q\sin\lambda\Theta', \tag{33}$$

where t is the acquisition period.

3.3.2. *Sequence 2*

In the case of the bi-selective inversion experiment the density matrices for the three sites after the mixing period are given as follows:

$$\sigma_{A,B}(\tau_m) = z_{1A,B}(\tau_m) = z_{1A,B} * U, \tag{34}$$

$$\sigma_C(\tau_m) = z_{1C}(\tau_m) = z_{1C} * V. \tag{35}$$

Here

$$U = 1 + \frac{1}{3}(\cos\lambda\Theta - 1)\exp[-(a+b)\tau_m] + \frac{2}{3}(\cos\lambda\Theta - 1)\exp[-(a-2b)\tau_m], \quad (36)$$

$$V = 1 - \frac{2}{3}(\cos\lambda\Theta - 1)\exp[-(a+b)\tau_m] + \frac{2}{3}(\cos\lambda\Theta - 1)\exp[-(a-2b)\tau_m]. \quad (37)$$

The final signals for a single crystal for both the inverted sites (A and B) are given as

$$S_{\mathrm{Inv,crystal}}(t) \propto \frac{\sqrt{3}}{2}\lambda U \sin\lambda\Theta'. \quad (38)$$

For the un-inverted site the final signal is given by

$$S_{\mathrm{Uninv,crystal}}(t) \propto \frac{\sqrt{3}}{2}\lambda V \sin\lambda\Theta'. \quad (39)$$

We should note here that the uninverted site (C) remains undetected in our experiments.

For a polycrystalline sample we need to take powder averages of the final signals according to Equation (10) in both selective and bi-selective experiments.

4. Experimental

Selective and bi-selective inversion recovery experiments were carried out with polycrystalline chloral hydrate [Cl_3C–$CH(OH)_2$] at a series of temperatures. The spectra were recorded with a Bruker Avance 400 NMR spectrometer (5.4 cm vertical magnet bore) using a Bruker 5 mm BBO probehead. The probe was mounted horizontally on the floor in a cardboard enclosure to protect against drafts, at a distance of 3.7 m from the centre of the Ultrashield^{TM} magnet to reduce the line broadening due to the stray field of the magnet. The sample temperature was measured and regulated using a Bruker variable temperature unit BVT-3200.

Chloral hydrate exhibits an essentially axially symmetric quadrupolar interaction ($\eta = 0$) [21] and reorientation about the C–C bond may be modelled as a three-site exchange. Three ^{35}Cl NQR lines are observed for this case [21,23]. The NQR frequencies at $T = 300$ K are $\nu_A = 38.750$ MHz, $\nu_B = 38.664$ MHz and $\nu_C = 37.476$ MHz [21]. The two lines that are 86 kHz apart from each other may conveniently be observed simultaneously within the maximum spectral window available on our instrument (150 kHz). NQR relaxation data recorded above 250 K confirm the occurrence of rotational jumps that interchange the three Cl atoms, resulting in a three-site exchange process [5,23].

Table 3. Pulse duration and corresponding power levels.

Pulse	Pulse width (μs)	Power level (dB)
Bi-selective 90°	70	~−3.2
Bi-selective 180°	150	~−4.0
Selective 180°	150	~2.2

The transmitter frequency (ν_T) was placed at the middle of the two lines ν_A and ν_B and expressed as $\nu_T = (\nu_A + \nu_B)/2$ and then the soft pulse envelope was amplitude modulated with the modulation frequency $\nu_m = (\nu_A - \nu_B)/2$. Here ν_A and ν_B are the NQR frequencies corresponding to sites A and B. This procedure was repeated for all temperatures investigated, since the resonance frequencies are temperature dependent, e.g. the line separation between ν_A and ν_B changes from 79 to 87 kHz over a temperature range of 15 to 35°C.

The cosine modulated bi-selective 90° pulse used as the read pulse was calibrated for maximum signal intensity while the selective and cosine modulated bi-selective 180° pulses were calibrated separately for null signal. Table 3 gives the pulse parameters used in the experiments.

Several series of experiments were carried out for various mixing periods ranging from 0 to 50 ms and at five different temperatures to extract the activation parameters. 128 data points were collected during the acquisition period. The number of scans was 32 and the repetition time was 250 ms. The total time of a single experiment is less than half a minute.

5. Results and discussion

In the case of chloral hydrate the reduction factor $r = -0.33$ as determined from the tetrahedral geometry of the reorienting Cl_3C– group [9]. Hence the fitting equations are derived for this value of r after taking the powder average of the terms containing $\lambda\Theta$ in the final signals given by Equations (32), (33), (38) and (39). The relevant fitting equations are given below. A notable point here is that the fitting equation for the un-inverted site in the case of the bi-selective inversion recovery experiment is not relevant for our study since the un-inverted site is well beyond the spectral window of our instrument under our operating conditions.

Selective experiment

Signal from the inverted site:

$$S_{\mathrm{Inv,powder}} = 0.75 - 0.806223\exp[-(a+b)\tau_{\mathrm{m}}] - 0.403116\exp[-(a-2b)\tau_{\mathrm{m}}]. \quad (40)$$

Signal from the un-inverted site:

$$S_{\mathrm{Uninv,powder}} = 0.75 + 0.403116\exp[-(a+b)\tau_{\mathrm{m}}] - 0.403116\exp[-(a-2b)\tau_{\mathrm{m}}]. \quad (41)$$

Bi-selective experiment

Signal from the inverted sites:

$$S_{\mathrm{Inv,powder}} = 0.75 - 0.403116\exp[-(a+b)\tau_{\mathrm{m}}] - 0.806223\exp[-(a-2b)\tau_{\mathrm{m}}]. \quad (42)$$

Signal from the un-inverted site:

$$S_{\mathrm{Uninv,powder}} = 0.75 + 0.806223\exp[-(a+b)\tau_{\mathrm{m}}] - 0.806223\exp[-(a-2b)\tau_{\mathrm{m}}]. \quad (43)$$

As a model of the mixing time dependence of the signal, we have plotted all the fitting equations against mixing time (0–50 ms) for chloral hydrate at $T = 300$ K, employing the following model parameters for the fitting equations: $k = 250\,\mathrm{s}^{-1}$, $T_1 = 3$ ms, $r = -0.33$ [21]. Figure 3 displays the theoretical plots of signal intensity of the inverted site versus mixing time (τ_{m}) at $T = 300$ K for chloral hydrate for the selective experiment as well as the bi-selective experiment. Figure 4 displays the theoretical plots of the signal intensity for the un-inverted site versus mixing time at various r values: Figure 4(a) for selective and Figure 4(b) for bi-selective inversion recovery experiments, respectively.

The general resemblance of these plots to that for NMR exchange or NMR cross-relaxation is notable. However, from Figure 4 we may conclude that the change in signal intensity of the un-inverted site in the case of chloral hydrate is only of the order of 5–6%. We were not able to detect this small change in intensity in our singly selective experiment.

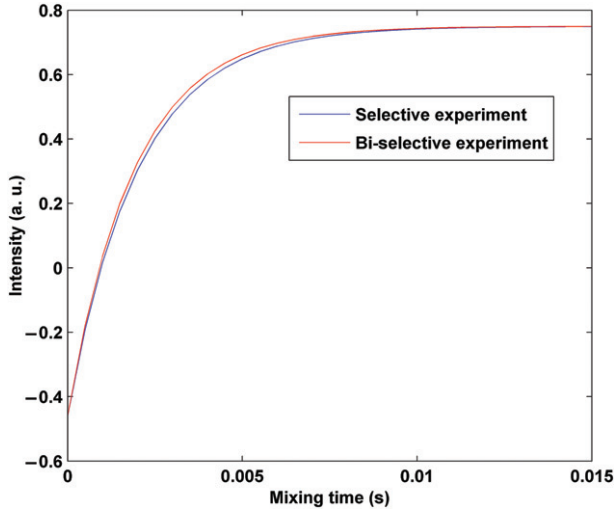

Figure 3. Theoretical plot of the signal intensity versus mixing time (τ_{m}) for the inverted site at $T = 300$ K and $r = -0.33$ for both the selective inversion and the bi-selective inversion experiments.

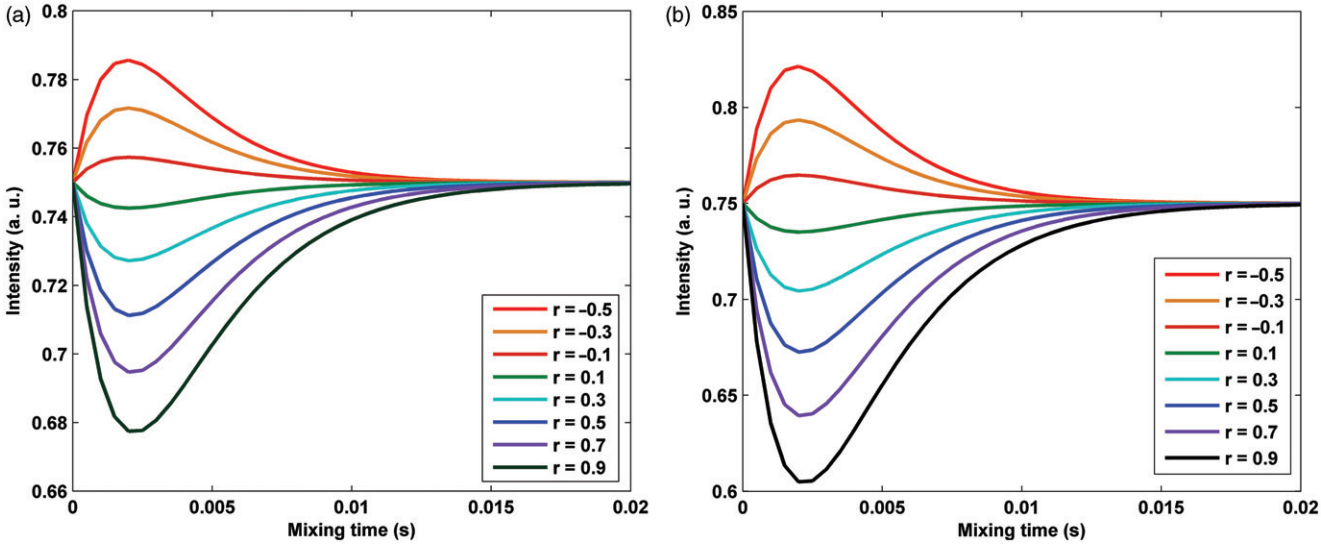

Figure 4. Theoretical plot of the signal intensity versus τ_{m} for the un-inverted site at $T = 300$ K for various r values: (a) selective inversion experiment, (b) bi-selective inversion experiment.

Figure 5 displays plots of experimental signal intensity versus τ_m for the bi-selective experiment at two different temperatures. Similar plots are obtained for the selective inversion experiment. The experimental plots at the five temperatures investigated were then fitted with the appropriate fitting equations. The kinetic parameters thus determined are tabulated in Tables 4 and 5.

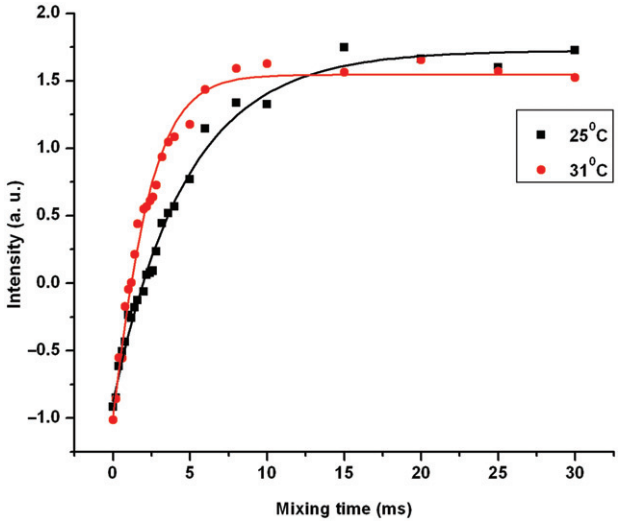

Figure 5. Plot of the experimental signal intensity of the high-frequency line versus τ_m for the bi-selective experiment at two different temperatures, $T = 298$ and 304 K.

Table 4. Kinetic parameters calculated from the experimental plot of signal intensity versus τ_m at various temperatures.

	Selective experiment		Bi-selective experiment	
Temperature (T) (K)	T_1 (ms)	k (s^{-1})	T_1 (ms)	k (s^{-1})
296	3.92	161.07	4.31	185.915
298	3.75	232.257	3.63	225.060
300	3.01	243.645	3.20	270.711
302	2.49	278.415	2.49	281.079
304	2.15	326.028	2.27	369.606

The results obtained are in good agreement with the previous values obtained by a recent 2D NQR exchange experiment [21]. It may be noted that we report in addition the corresponding activation parameters in terms of the Eyring plot.

6. Conclusion

In this study we have demonstrated that both the 1D 'bi-selective inversion recovery experiment' and the 1D 'selective inversion recovery experiment' are suitable for the study of dynamic processes in the solid state by pulsed NQR spectroscopy.

Since the NQR spectrum is spread over several kHz, off-resonance effects play a critical role in influencing excitation efficiency and sensitivity. The 1D 'bi-selective inversion recovery' sequence presented here achieves simultaneous two-site excitation, which avoids the formidable off-resonance effect. Secondly, it guarantees that the exchanging sites will be equally affected by pulse non-idealities. Similarly, the selective version also avoids the off-resonance effect and achieves a much better selectivity in exciting a particular NQR line when compared with an on-resonance hard or soft rectangular pulse.

Compared with the 2D NQR exchange experiment, both our 1D sequences save a great deal of experiment time and provide a clear definition of the time window during which the dynamic process occurs. In the 2D experiments reported the maximum evolution time often becomes comparable to the mixing time [21]; in our sequences, on the other hand, besides the absence of the evolution period, the soft pulse durations (tens of μs) are also much shorter compared with the mixing time (a few ms).

These 1D experiments may be readily carried out at a large number of values of the mixing time and the resulting signal amplitudes plotted versus the mixing time to infer the relevant rate constants accurately. Both our experiments thus enable accurate measurements of the spin-lattice relaxation rate and exchange rate at a given temperature. With a set of variable temperature measurements, the kinetic as well as

Table 5. Activation parameters obtained for the reorientation process.

	Arrhenius plot		Eyring plot	
Experiment	Activation energy (E_a) ($kJ\,mol^{-1}$)	Frequency factor (A) (s^{-1})	Enthalpy of activation (ΔH^*) ($kJ\,mol^{-1}$)	Entropy of activation (ΔS^*) ($J\,mol^{-1}\,K^{-1}$)
Selective	56.728	1.833×10^{12}	54.371	−18.055
Bi-selective	57.357	2.529×10^{12}	54.909	−15.678

activation parameters are readily obtained; in the case of chloral hydrate, these are in good agreement with recent literature values [21]; it should be noted that we report, in addition, the corresponding activation parameters in terms of the Eyring plot.

The application of our NQR approach to a variety of other chlorine-containing molecules in the solid state is in progress in our laboratory.

Acknowledgements

SP has great pleasure in acknowledging CSIR, India, for the grant of a Senior Research Fellowship. The authors gratefully acknowledge a spectrometer grant to the Department of Chemistry from DST, India.

References

[1] S. Alexander and A. Tzalmona, Phys. Rev. A **138**, 845 (1965).
[2] H. Chihara and N. Nakamura, in *Advances in Nuclear Quadrupole Resonance*, edited by J.A.S. Smith (Heyden, London, 1980).
[3] M. Buyle-Budin, Ann. Phys. (Paris) **10**, 533 (1955).
[4] D.E. Woessner and H.S. Gutowsky, J. Chem. Phys. **39**, 440 (1963).
[5] N.E. Ainbinder, B.F. Amirkhanov, I.V. Izmest'ev, *et al.*, Sov. Phys. Solid State **13**, 344 (1971).
[6] H.S. Gutowsky and D.W. McCall, J. Chem. Phys. **32**, 548 (1960).
[7] E. Rommel, P. Nickel, F. Rohmer, *et al.*, Z. Naturforsch., Teil A **47**, 382 (1992).
[8] P. Nickel and R. Kimmich, J. Molec. Struct. **345**, 253 (1995).
[9] N. Sinyavsky, N. Velikite, and M. Maćkowiak, Molec. Phys. **99**, 1653 (2001).
[10] M. Maćkowiak, N. Sinyavsky, and B. Blümich, J. Molec. Struct. **743**, 53 (2005).
[11] M. Maćkowiak, Acta Phys. Pol. A **108**, 61 (2005).
[12] J. Jeener, B.H. Meier, P. Bachmann, *et al.*, J. Chem. Phys. **71**, 4546 (1979).
[13] V. Vimalan, S. Pal and N. Chandrakumar, presented at the 21st ICMRBS/NMRS, Hyderabad, India, 2005 (unpublished).
[14] S. Pal and N. Chandrakumar, presented at the Mid Year Meeting-CRSI, IIT-Madras, Chennai, India, 2006 (unpublished).
[15] G.W. Leppelmeir and E.L. Hahn, Phys. Rev. **142**, 179 (1966).
[16] M. Goldman, *Advances in Magnetic Resonance: The Waugh Symposium* (Academic Press, San Diego, CA, 1990).
[17] S.Z. Ageev and B.C. Sanctuary, Chem. Phys. Lett. **225**, 499 (1994).
[18] C. Schurrer and S.C. Pérez, Appl. Magn. Reson. **16**, 135 (1999).
[19] E. Harel and H. Cho, J. Magn. Reson. **183**, 308 (2006).
[20] M. Bloom, E.L. Hahn, and B. Herzog, Phys. Rev. **97**, 1699 (1955).
[21] N. Sinyavsky, M. Maćkowiak and B. Blümich, Z. Naturforsch. **57a**, 53 (2002).
[22] H.M. McConnell, J. Chem. Phys. **28**, 430 (1958).
[23] H. Chihara and N. Nakamura, Bull. Chem. Soc. Japan **45**, 3530 (1972).